DMO processing for mode-converted waves in a medium with a linear increase in velocity with depth

Shaowu Wang, John C. Bancroft, and Don C. Lawton

ABSTRACT

Dip moveout (DMO) processing for converted-waves (*P-SV*) differs from that for either *P*- or *S*-waves only because of the asymmetry of down-going and up-going raypaths, even in an isotropic and homogeneous medium and with a zero-dip reflector. This makes the kinematics more complicated than that for *P*-waves or *S*-waves. Previous work on DMO processing for a depth-variable velocity medium has been concerned with DMO processing for either *P*- or *S*-waves.

In this paper, an analytical expression for the *P-SV* DMO operator in a medium with a vertical, linear velocity gradient is derived. The differences between DMO operators in constant velocity medium and a linear velocity gradient medium are discussed. Finally, an approximate operator for a linear velocity gradient medium is proposed, and we show that this operator fits the accurate operator very well, making the *P-SV* DMO processing in a depth-variable velocity medium practical.

INTRODUCTION

Dip-moveout (DMO) analysis in a medium of constant velocity is well understood and is readily implemented when dealing only with either *P*-waves or *S*-waves (Hale,1984). DMO processing tries to overcome the reflection point dispersion associated with dipping events.

DMO processing for converted-waves differs from normal (*P-P* or *S-S*) waves because of the asymmetry of down-going and up-going raypaths, even in an isotropic and homogeneous medium and with zero-dip reflector. This makes the kinematics more complicated than that for normal waves. Harrison (1990, 1992) proposed exact integral solutions for the DMO processing for converted-waves in a constant velocity medium. Alfaraj and Larner (1991) extended Gardner DMO method to converted-waves by transforming (t, x) domain into (t_1, k) domain in which the relationship between time t_1 and offset k is hyperbolic and dip-independent. Based on the hyperbolic approximation to the converted-wave DMO expression, an approximate DMO processing method for mode-converted waves in the frequency-wavenumber (f-k) domain was proposed by Alfaraj (1992).

DMO processing for a depth-variable velocity medium has been discussed by many authors (e.g., Perkins and French, 1990; Artley,1991; Dietrich and Cohen, 1992), but, their work was concerned mainly with DMO processing for either *P*-waves or *S*-waves. Harrison (1992) tried to adapt the DMO operator for a constant velocity medium to fit the layered velocity model by using approximations.

In this paper, an analytical expression for a *P-SV* DMO operator in a medium with linear velocity gradient is derived, then the differences of DMO operators in

constant velocity medium and linear velocity gradient medium are discussed. Finally, an approximate DMO operator for a linear velocity gradient medium is proposed.

DERIVATION OF THE DMO OPERATOR FOR A LINEAR VELOCITY GRADIENT

Figure 1 shows *P*-wave energy being mode-converted by a dipping reflector and recorded by a multicomponent receiver in a medium with a linear velocity gradient.

S: Source position;

R: Receiver position;

C: Conversion point;

P: Position of the conversion point on the surface;

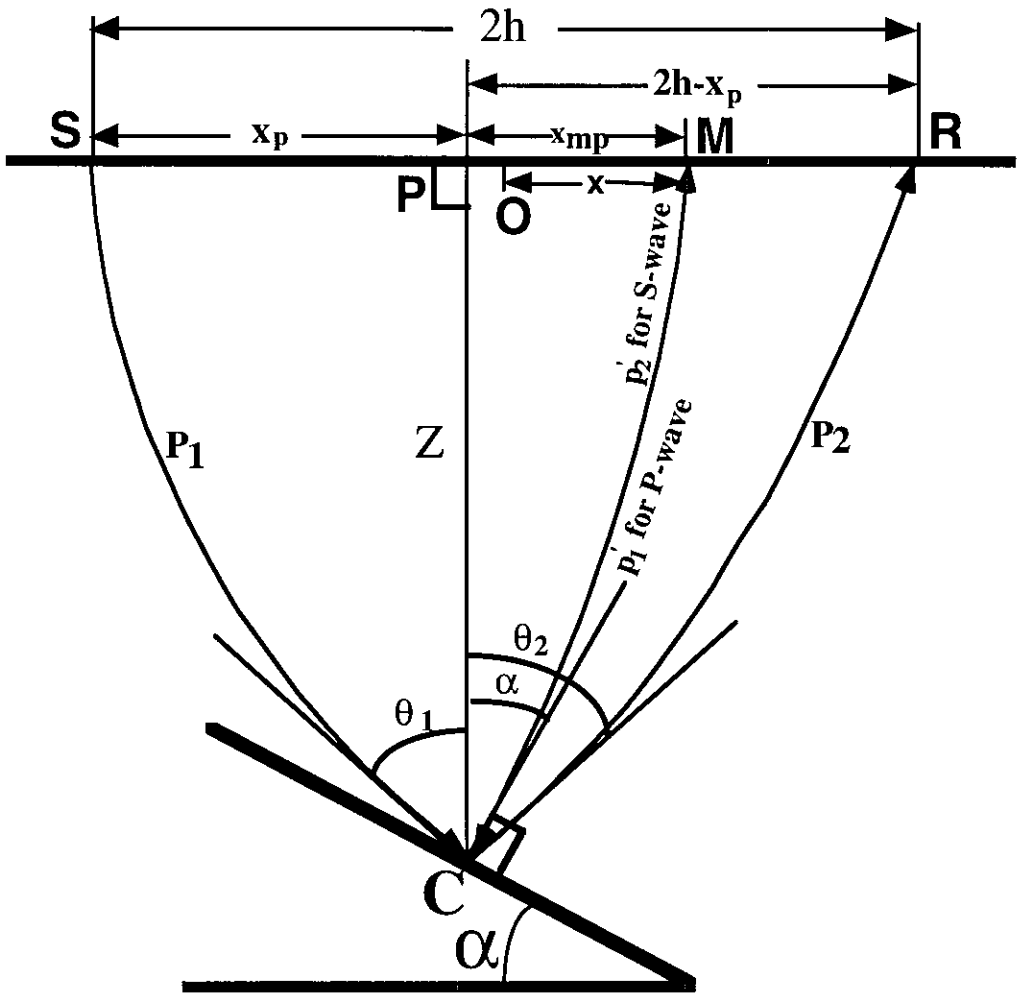

FIG. 1. Generating the zero-offset response for constant velocity gradient medium

M: Zero offset position;

O: Middle point between S and R;

$p_1 = \frac{\sin\theta_1}{V_{p(z)}}$: Ray parameter for *P*-wave;

$p_2 = \frac{\sin\theta_2}{V_{s(z)}}$: Ray parameter for *S*-wave;

The velocity along path SC is $V_{p(z)}$ and the velocity along CR is $V_{s(z)}$. For the constant velocity gradient model, they are

$$V_p \equiv V_{p(z)} = V_{p0} + k\,z, \tag{1a}$$

$$V_s \equiv V_{s(z)} = V_{s0} + \frac{k}{\gamma} z, \tag{1b}$$

where V_{p0} and V_{s0} are *P*- and *S*-wave velocities at the surface respectively. $V_{p(z)}$ and $V_{s(z)}$ are the velocities of *P*-waves and *S*-waves at the depth Z and denoted as V_p and V_s for convenience. The velocity gradient is given by k, and the V_p/V_s ratio is given by γ. In order to simplify the derivation while not losing the general application of the conclusions, γ is assumed to be constant, i.e.,

$$V_p/V_s = \gamma(\text{constant}). \tag{2}$$

According to Snell's law, the travel time t_{sc} for *P*-waves from source S to conversion point C is

$$t_{SC} = \int_0^z \frac{d_z}{V_p\sqrt{1-p_1^2V_p^2}} = \frac{1}{k}\int_{V_{p0}}^{V_{p0}+kz} \frac{dV_p}{V_p\sqrt{1-p_1^2V_p^2}} \qquad k\neq 0$$

$$= \frac{1}{k} log\left[\left(\frac{V_p}{V_{p0}}\right)\frac{1+\sqrt{1-p_1^2V_{p0}^2}}{1+\sqrt{1-p_1^2V_p^2}}\right]. \tag{3}$$

In the same way as above, the travel time t_{CR} for *S*-waves from conversion point C to receiver R is

$$t_{CR} = \frac{\gamma}{k} log\left[\left(\frac{V_s}{V_{s0}}\right)\frac{1+\sqrt{1-p_2^2V_{s0}^2}}{1+\sqrt{1-p_2^2V_s^2}}\right]. \tag{4}$$

The total travel time t is given by

$$t=t_{SC}+t_{CR}. \tag{5}$$

Substituting for t_{SC} and t_{CR} from equations (3) and (4) into equation (5) and simplifying it gives:

$$e^{kt} = \left(\frac{V_p}{V_{p0}}\right)\frac{1+\sqrt{1-p_1^2V_{p0}^2}}{1+\sqrt{1-p_1^2V_p^2}}\left[\left(\frac{V_s}{V_{s0}}\right)\frac{1+\sqrt{1-p_2^2V_{s0}^2}}{1+\sqrt{1-p_2^2V_s^2}}\right]^{\gamma}. \tag{6a}$$

Using a similar approach, the horizontal distances from S to C (for *P*-waves) and from C to S (for *S*-waves) can be derived as following

$$X_p = \frac{\sqrt{1-p_1^2V_{p0}^2}-\sqrt{1-p_1^2V_p^2}}{kp_1},$$

$$2h-X_p = \gamma\frac{\sqrt{1-p_2^2V_{s0}^2}-\sqrt{1-p_2^2V_s^2}}{kp_2}.$$

Solving the above equations and express p_1 and p_2 as the function of V_p *or* V_s, we get:

$$p_1 = \frac{2X_pk}{\sqrt{\left(X_p^2k^2+V_{p0}^2+V_p^2\right)^2-4V_p^2V_{p0}^2}}, \tag{6b}$$

$$p_2 = \frac{2(2h-X_p)k}{\gamma\sqrt{\left((2h-X_p)^2\left(\frac{k}{\gamma}\right)^2+V_{s0}^2+V_s^2\right)^2-4V_s^2V_{s0}^2}}. \tag{6c}$$

From the equations (2) and (6), p_1, p_2 and v_p(or z) can be calculated for given offset X_p from the source and two-way travel time t.

The dip angle α can then be computed from the two ray parameters p_1 and p_2. Referring to Figure 1, it is seen that

$$p = \frac{sin\ (\theta_1+\alpha)}{V_p} = \frac{sin\ (\theta_2-\alpha)}{V_s},$$

where p is the ray parameter for at the mode-conversion position on the dipping interface. Expanding the above equation and simplifying it, sin α can be expressed as

$$sin\ \alpha = \frac{p_2-p_1}{\sqrt{\left(\frac{1}{V_p}\sqrt{1-p_1^2V_p^2}+\frac{1}{V_s}\sqrt{1-p_2^2V_s^2}\right)^2+(p_2-p_1)^2}}. \tag{7}$$

From the above equation, we can see that when $p_2 \geq p_1$, α is positive; when $p_2 \leq p_1$, α is negative.

The DMO curves are made by constructing the zero-offset response. Figure 1 has been drawn to indicate that the zero-offset down-going and up-going raypaths are coincident. This is true only for constant γ value (Harrison, 1992). Due to the assumption in equation (2), the *P*-wave and *S*-wave ray parameters can be expressed as

$$p_1' = \frac{\sin\alpha}{V_p},$$

$$p_2' = \frac{\sin\alpha}{V_s}.$$

Then, just as the derivation of the two-way travel time t, the zero-offset two-way travel time τ can be derived as

$$\tau = \frac{1}{k}\log\left\{\left(\frac{V_p}{V_{p0}}\right)^{\frac{1+\sqrt{1-\sin^2\alpha\left[\frac{V_{p0}}{V_p}\right]^2}}{1+\cos\alpha}}\left[\left(\frac{V_s}{V_{s0}}\right)^{\frac{1+\sqrt{1-\sin^2\alpha\left[\frac{V_{s0}}{V_s}\right]^2}}{1+\cos\alpha}}\right]^{\gamma}\right\}. \tag{8a}$$

The offset X_{mp} from the point of mode conversion C in Figure 1, must be the same for down-going and up-going zero-offset raypaths, i.e.,

$$X_{mp} = \frac{\sqrt{1-p_1'^2V_{p0}^2}-\sqrt{1-p_1'^2V_p^2}}{kp_1'} = \frac{\sqrt{V_p^2-\sin^2\alpha V_{p0}^2}-V_p\cos\alpha}{k\sin\alpha}, \tag{8b}$$

The midpoint-offset of the DMO operator X is then given by

$$X = X_p + X_{mp} - h. \tag{8c}$$

Equations (8) are used to generate the shape of the DMO response.

IMPLEMENTATION OF *P-SV* DMO FOR A MEDIUM WITH A LINEAR VELOCITY GRADIENT

If an integral-summation algorithm (Deregowski, 1985) is implemented, the algorithm consists of first constructing a time domain DMO response for each input trace, then summing the response to get the final DMO-corrected output. In the implementation, dip aperture width, amplitude and phase corrections of the operator must be discussed.

Aperture width and maximum dip limit

Equations (8) are used to generate the shape of the DMO curves, but it is still necessary to determine their maximum physical extents. These extents establish the maximum aperture width, corresponding to some maximum physical dip. In turn, given the maximum physical dip to be dealt with, the corresponding aperture width is determined.

In equation (7), α is actually the physical dip. If we let

$$|\sin \alpha| \leq |\sin \alpha_{max}|,$$

where α_{max} is the maximum physical dip, then the maximum aperture width can be determined. The smaller the α_{max}, then the smaller will be the aperture width. Small aperture prevents spatial aliasing, suppresses the steeply dipping coherent noise, and saves run-time for DMO processing.

Amplitude and phase corrections of the *P-SV* DMO operator

To assess the effect of the DMO operator on the input data, it is necessary to analyze how the data are changed by summation across the operator width, which generates the final DMO-corrected output. According to Harrison (1992), if the gain G_0 at the zero-dip conversion point, where the curvature is C_0 , is defined as

$$G_0 = \sqrt{f C_0},$$

where f is the frequency. The gain at any point along the DMO curve will then be

$$G = \sqrt{\frac{C}{C_0}} G_0,$$

where C is the curvature at that point.

An asymptotic -45 degree phase correction is applied in the implementation to test the DMO operator.

APPROXIMATIONS OF DMO OPERATOR

It has not been possible to determine an explicit solution of τ with respect to offset X from the mid-point, so there is a disadvantage in run-time to generate the shape of the DMO response. However, for constant velocity DMO (Harrison, 1990, 1992), the zero-offset travel time τ can be explicitly expressed as the function of X, i.e.,

$$\tau = \frac{V_p^a + V_s^a}{V_p^a V_s^a} \sqrt{(h^2 - X^2)\left(\frac{V_p^{a2} V_s^{a2} t^2}{2h\left(V_p^{a2}(h-X) + V_s^{a2}(h+X)\right)} - 1\right)}, \tag{9}$$

where V_p^a and V_s^a are the approximated velocities for *P*- and *S*-waves respectively. If we try to use the constant velocity DMO operator for depth-variable velocity model, then we must find a proper velocity approximation to make the approximated operator fit the accurate operator. Harrison (1992) pointed out that the average *P*- and *S*-wave velocities at the depth of zero-dip conversion point are the best velocities to use in the construction of the DMO response. In this paper, it is shown that both average velocity and RMS velocity at the depth of the conversion point, at which zero-offset travel time is calculated, are very good velocity approximations for using equation (9) in the construction of DMO response.

For a medium with a linear velocity gradient as expressed in equation (1), the RMS velocity can be derived as

$$V_p^{RMS} = \left(\frac{1}{t} \int_0^t V_{(t)}^2 d_t \right)^{1/2} = \left(\frac{kzV_{p0} + \frac{k^2 z^2}{2}}{log\left(1 + \frac{k}{V_{p0}} z\right)} \right)^{1/2}, \tag{10}$$

and the average velocity can be obtained as

$$V_p^{Ave} = \frac{1}{t} \int_0^t V_{(t)} d_t = \frac{kz}{log\left(1 + \frac{k}{V_{p0}} z\right)}, \tag{11}$$

From the equations (10) and (11), V_p^{RMS} and V_p^{Ave} are the functions of depth z at the conversion point C, as denoted in Figure 2.

We have yet to know the depth z in order to obtain the RMS velocity or average velocity at that point. In the constant velocity model, there are following relationships

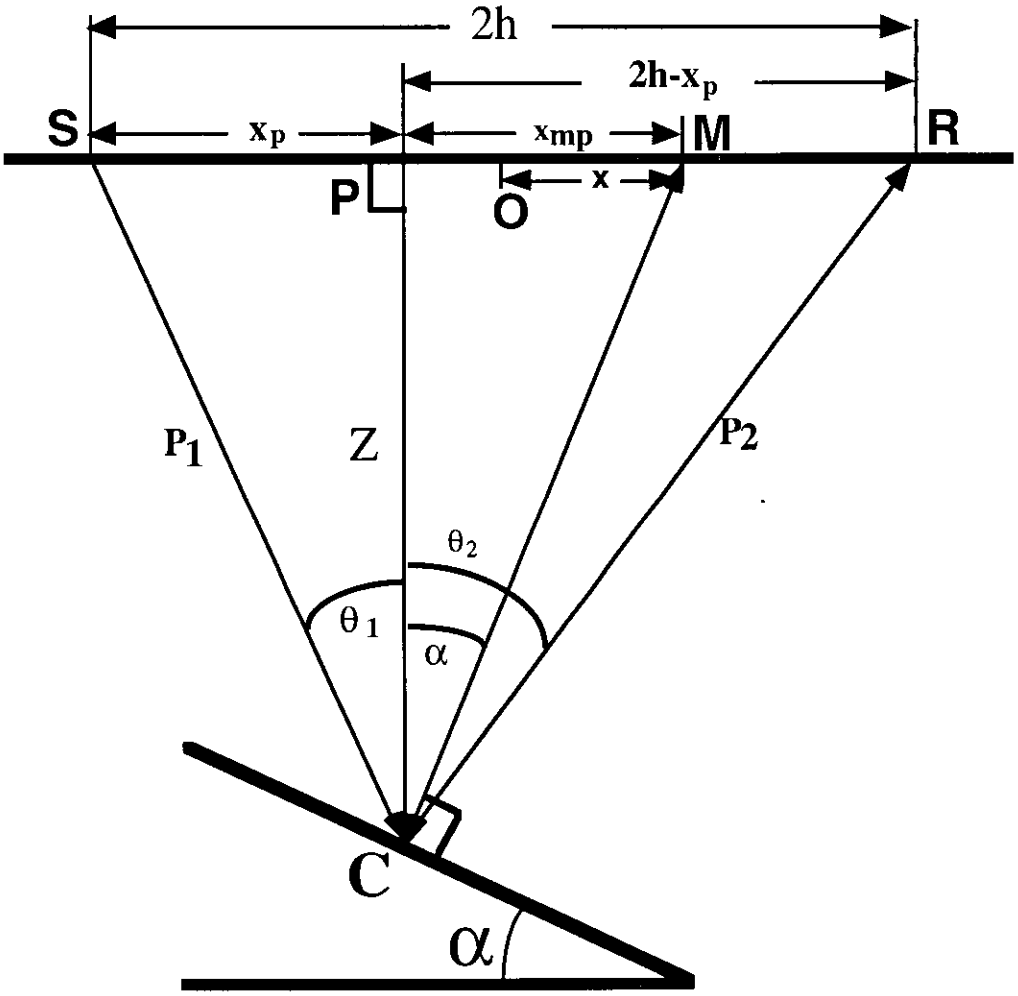

FIG. 2. Generating the zero-offset response for constant velocity medium

(Harrison, 1992):

$$2h = \sqrt{\left(\frac{V_p^a t}{\gamma^2\left(\frac{h-X}{h+X}\right)+1}\right)^2 - z^2} + \sqrt{\left(\frac{\gamma V_p^a t}{\gamma^2+\left(\frac{h+X}{h-X}\right)}\right)^2 - z^2}\,, \tag{12}$$

in which, V_p^a is the approximated velocity for P-waves. In this paper, it is the RMS velocity V_p^{RMS} or average velocity V_p^{Ave}.

Using equations (12), coupled with equation (10) or equation (11), the RMS velocity or average velocity can be calculated.

DISCUSSION

Figures 3 and 4 show that the shapes of the DMO trajectories for constant velocity medium and a linear velocity gradient medium are similar. The DMO trajectories shift to a later time along the zero-offset travel time (τ) axis and the curvatures become larger with the increase of velocity gradient k. If the ratio of P-wave velocity and S-wave velocity is constant, the positions of the zero-dip conversion points of constant velocity model and linear velocity gradient model are the same at a given depth. For the same physical dip limit, the aperture width is obviously reduced as k increases. This means that if the same DMO aperture width is used, the ability to deal with the steeply dipping events will be increased with an increasing velocity gradient k increases. Compared with the aperture width in Figure 4, in which the maximum physical dip angle α_{max} is 80 degrees, the aperture width in Figure 5 with α_{max} equal to 40 degrees is obviously reduced. In Figures 4 and 5, amplitude and phase corrections of the P-SV DMO operator were applied. From the comparison of Figure 4 with Figure 6, it was also found that with the increasing offset, the response seems to shift to a later time and the aperture width is proportionally increased for the same physical dip limit.

Figure 7 shows the curves of interval, RMS and average velocities calculated using equations (1a), (10) and (11) respectively. It is seen that RMS velocity and average velocity are very close for a medium k value. Even when depth z is as large as 10,000 m and velocity gradient k is 0.8, the difference between the RMS velocity and average velocity is less than 10%. But because average velocity is smoother than the RMS velocity, it is often preferred in practice.

DMO curves, using the average (dash-dot line) and RMS (dash line) velocities at the depth of zero-dip conversion point as the velocity approximation in constant velocity DMO operator discussed by Harrison (1992), and the accurate DMO curves discussed in this paper (solid line), are shown in Figures 8 and 9. Here, the accurate DMO curves are referring to the DMO curves calculated using the analytical formula (equations 8) without any approximations. The dash-dot lines (average velocity approximation) overlap the dash lines (RMS velocity approximation). This means the error due to the use of different velocity approximation is negligible, because the difference between RMS velocity and average velocity is small, and more importantly, unlike migration, the accuracy of DMO processing is fairly insensitive to velocity error. For small velocity gradient (Figure 8), the approximate DMO curves fit the accurate curves very well, but the velocity gradient increases, this match becomes worse, especially as the horizontal position of DMO operator from zero-dip conversion point

(Figure 9) increases. In the generation of the approximate DMO curves, ray bending was not taken into account and the aperture width of the approximate DMO curves is much wider than that of the accurate DMO curves.

The DMO curves for the velocity approximations discussed in this paper are shown in Figure 10, in which the approximate velocities are the RMS velocity and average velocity at the depth of the conversion point, rather than at the depth of zero-dip conversion point. Compared with the DMO curves shown in Figure 9, the DMO curves with new velocity approximations fit the accurate DMO curves very well. For the same reason discussed above, the aperture width of the approximate operator is wider than that of the accurate operator. If the maximum dip angle of the approximate operator is limited to 45 degrees, as shown in Figure 11, while the maximum dip angle of the accurate operator is still 80 degree, the aperture widths for the approximate operators and accurate operator are very close. Based on this discussion, a very important property about DMO processing for linear velocity gradient medium can be obtained. In the use of the approximate DMO operator with new velocity approximation, we can use a DMO operator with 45 degree maximum dip angle to DMO-correct an event with an 80 degree physical dip angle. This will help to reduce run-time, prevent spatial aliasing and suppress steeply dipping coherent noise.

CONCLUSIONS

An analytical expression for the *P-SV* DMO operator in a medium with linear velocity gradient was derived and the differences of DMO operators between constant velocity medium and linear velocity gradient medium were discussed. It is shown that with an increase in velocity gradient, the aperture width of the DMO operator becomes smaller. The presence of ray bending is seen to enhance the steep-event accuracy of the DMO result.

RMS and average velocities for the linear velocity gradient medium are very close, even when the velocity gradient and/or the depth is large. The accuracy of DMO processing is fairly insensitive to the velocity error. Due to these two properties, there is almost no difference between using the RMS velocity and using the average velocity as the velocity approximation in the generation of the DMO response for the constant velocity DMO operator.

Compared with the average or RMS velocity at the depth of zero-dip conversion point, the average velocity or RMS velocity at the depth of conversion point at which zero-offset travel time is calculated is a better velocity approximation used in the generation of DMO response using constant velocity DMO operator. Even with large offset, in fast varying velocity medium and in later time, the approximated DMO operator with new velocity approximation can fit the accurate operator very well.

Some of the methods discussed in this paper may be suitable for conventional *P*-wave DMO processing in the linear velocity gradient medium and the derivations of the accurate DMO operator for linear velocity gradient medium may be extended to the discussion of 3-D converted-wave DMO correction for the linear velocity gradient case.

ACKNOWLEDGMENTS

The authors would like to thank the sponsors of The CREWES Project.

REFERENCES

Alfaraj, Mohammed and Ken Larner, 1991, Dip moveout for mode-converted waves: Expanded Abstract of Technical Program, SEG 61, Houston, TX

Alfaraj, Mohammed, 1992, Transformation to zero offset for mode-converted waves by Fourier transformation, Expanded Abstract of Technical Program, SEG 62, New Orleans

Atley, Graig T., 1991, dip-moveout processing for depth-variable velocity: Expanded Abstract of Technical Program, SEG 61, Houston, TX

Deregowski, S. M., 1982, Dip moveout and reflector point dispersal: Geophysical Prospecting, 30, 318-322

Dietrich, Michel and Jack K. Cohen, 1992, 3-D migration to zero offset for a constant velocity gradient: an analytical formulation: Geophysical Prospecting, 41, 621-643

Godfrey, Robert J., 1992, DMO and V(z): Expanded Abstract of Technical Program, SEG 62, New Orleans

Hale, D., 1984, Dip-moveout by Fourier Transformation: Geophysics, 49, 741-757

Hale, D. and Craig Artley, 1993, squeezing dip-moveout for depth-variable velocity: Geophysics, 58, 257-264

Harrison, M., 1990, Converted wave DMO: Expanded Abstract of Technical Program, SEG 60, San Fransisco, CA

Harrison, M., 1992, Processing of *P-SV* surface-seismic data: Anisotropy analysis, dip moveout, and migration. Ph.D. thesis, The University of Calgary

Larner, Ken, Beasley, C. J. and Lynn, W., In question of the flank: Geophysics, 54, 701-717

Perkins, W. T. and W. S. French, 1990, 3-D migration to zero offset for a constant velocity gradient: Expanded Abstract of Technical Program, SEG 60, San Fransisco, CA

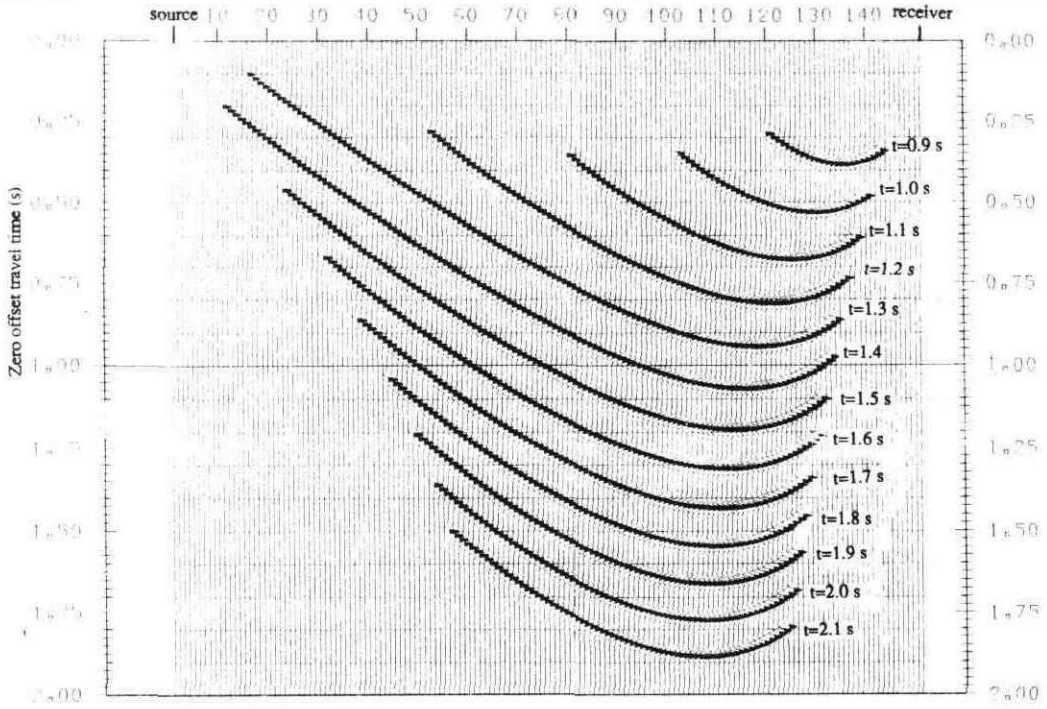

FIG. 3. *P-SV* DMO response for constant velocity medium without amplitude and phase corrections. The time indicated for each DMO curve is two-way travel time. V_{p0}=3000 m/s, V_{s0}=1500 m/s, 2h=2000 m, $\alpha_{max}=80^0$

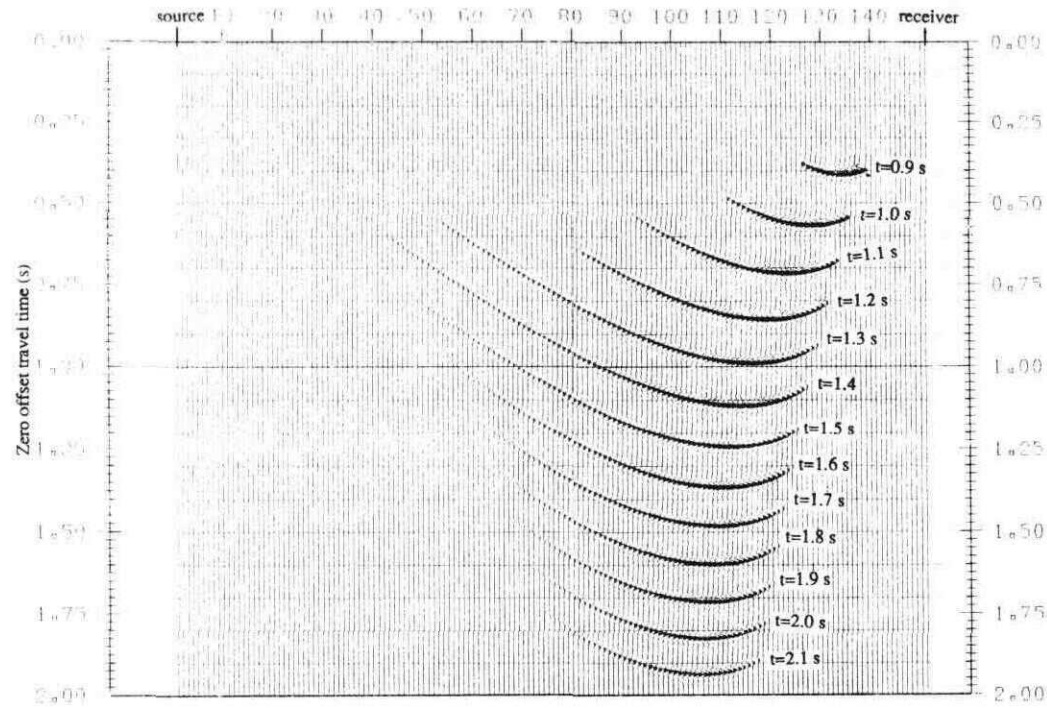

FIG. 4. *P-SV* DMO response for constant velocity gradient medium with amplitude and phase corrections. The time indicated for each DMO curve is two-way travel time. V_{p0}=3000 m/s, V_{s0}=1500 m/s, 2h=2000 m, $\alpha_{max}=80^0$ and k=0.4.

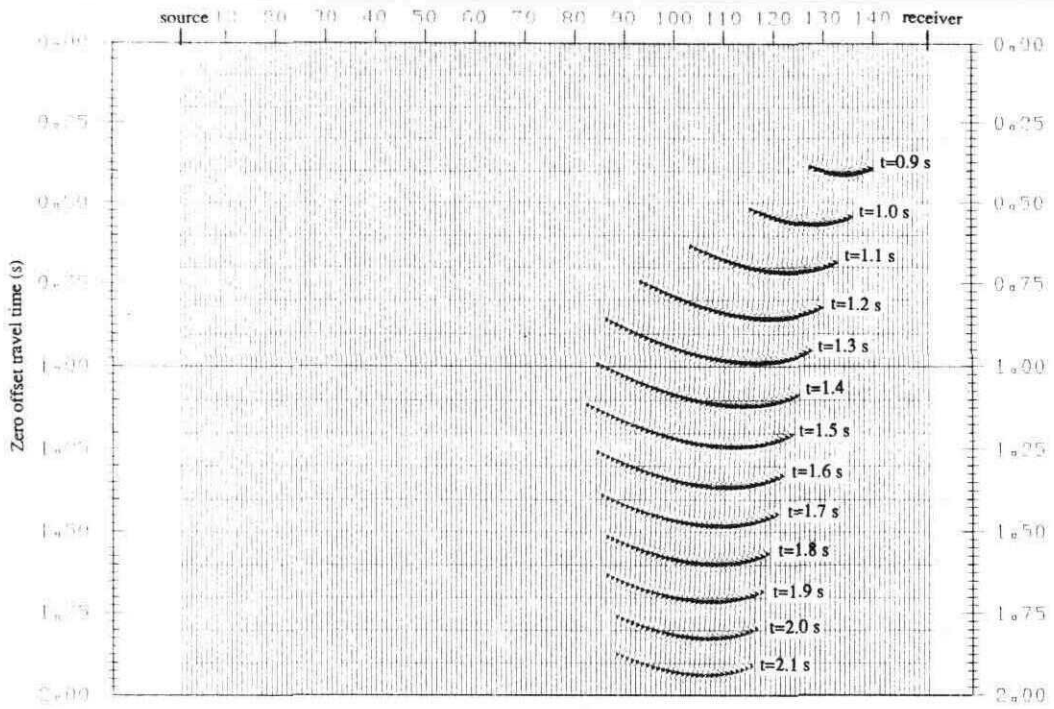

FIG. 5. *P-SV* DMO response for constant velocity gradient medium with amplitude and phase corrections. The time indicated for each DMO curve is two-way travel time. V_{p0}=3000 m/s, V_{s0}=1500 m/s, 2h=2000 m, $\alpha_{max}=40^0$ and k=0.4.

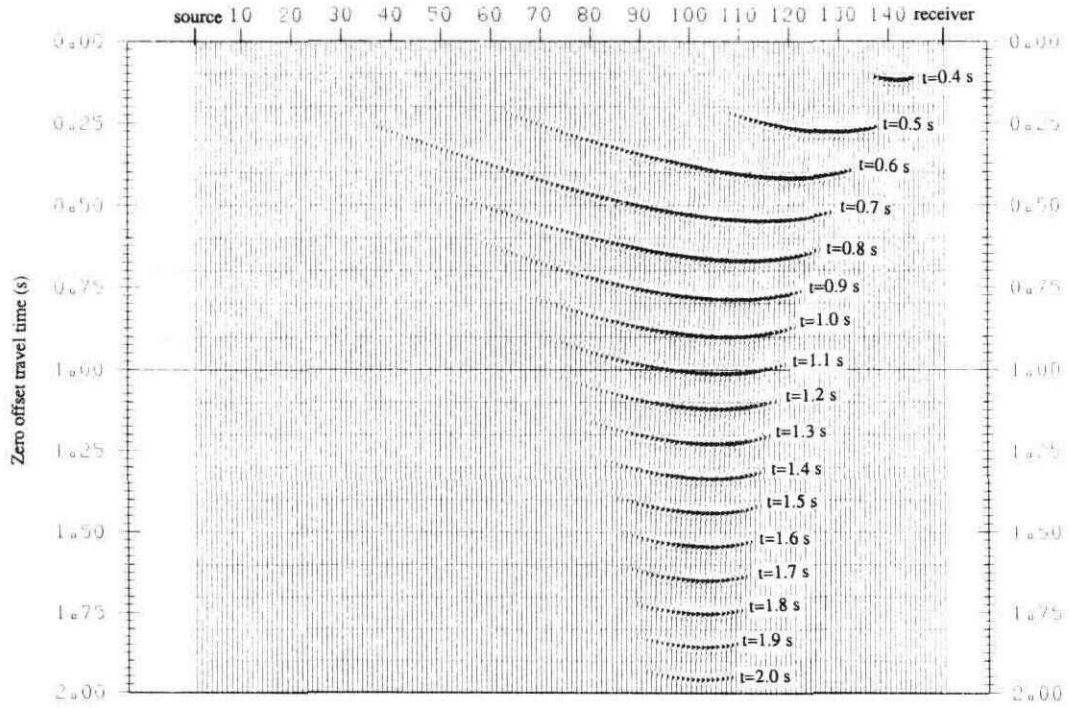

FIG. 6. *P-SV* DMO response for constant velocity gradient medium with amplitude and phase correction. The time indicated for each DMO curve is two-way travel time. V_{p0}=3000 m/s, V_{s0}=1500 m/s, 2h=1000 m, $\alpha_{max}=80^0$ and k=0.4.

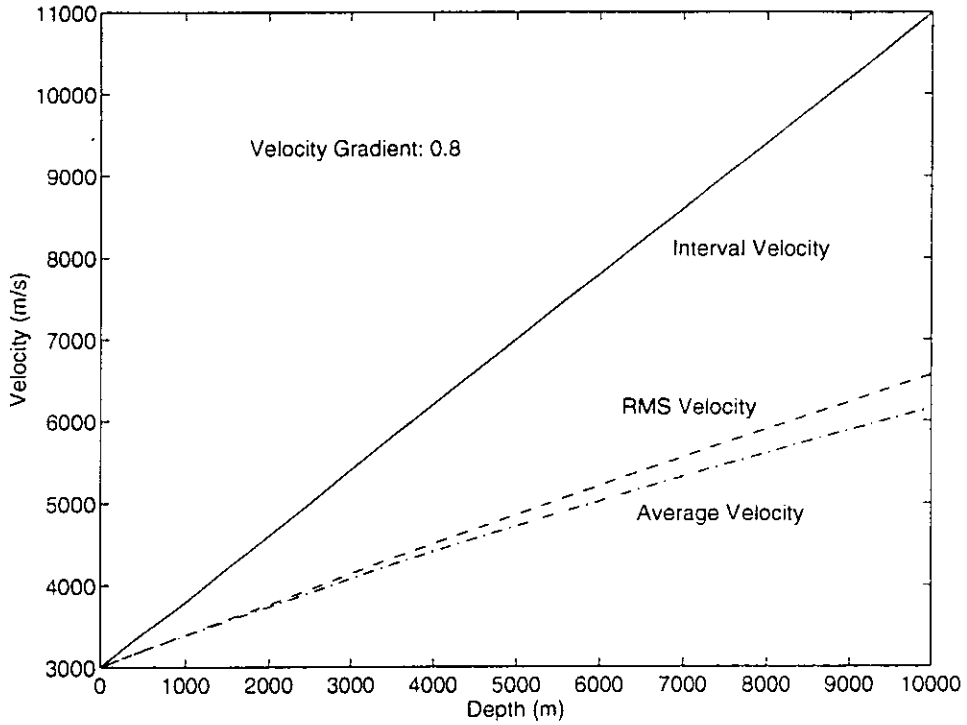

FIG. 7. The curves showing the relationship of interval, RMS and average velocities for constant velocity gradient model with velocity gradient: 0.8.

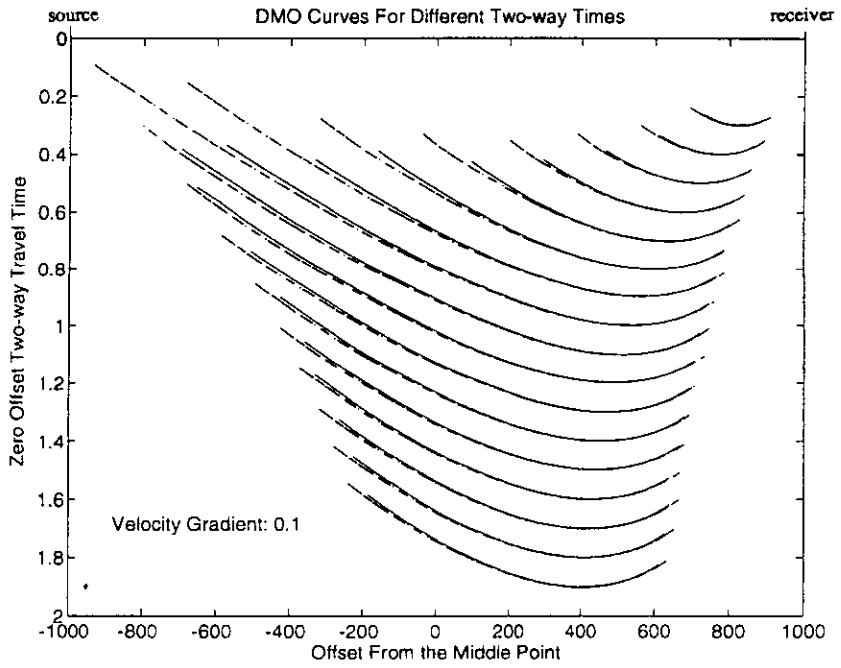

FIG. 8. *P-SV* DMO curves calculated using constant velocity DMO operator with approximated RMS (dash lines) and average (dash-dot lines) velocities at the depth of zero-dip conversion point, as suggested by Harrison. Solid lines are for accurate DMO operator. V_{p0}=3000 m/s, V_{s0}=1500 m/s, 2h=2000 m, $\alpha_{max}=80^0$ and k=0.1

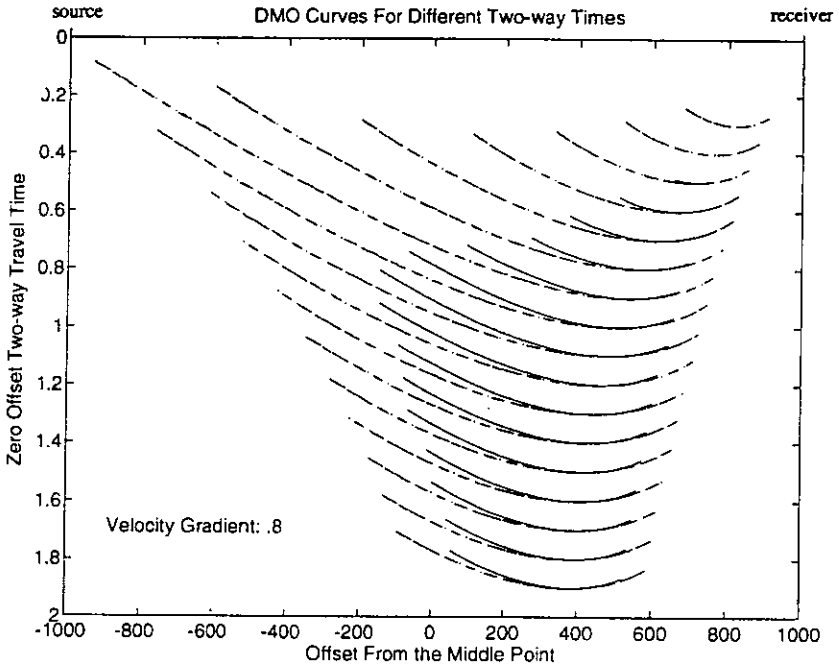

FIG. 9. *P-SV* DMO curves calculated using constant velocity DMO operator with approximated RMS (dash lines) and average (dash-dot lines) velocities at the depth of zero-dip conversion point, as suggested by Harrison. Solid lines are for accurate DMO operator. V_{p0}=3000 m/s, V_{s0}=1500 m/s, 2h=2000 m, $\alpha_{max}=80^0$ and k=0.8

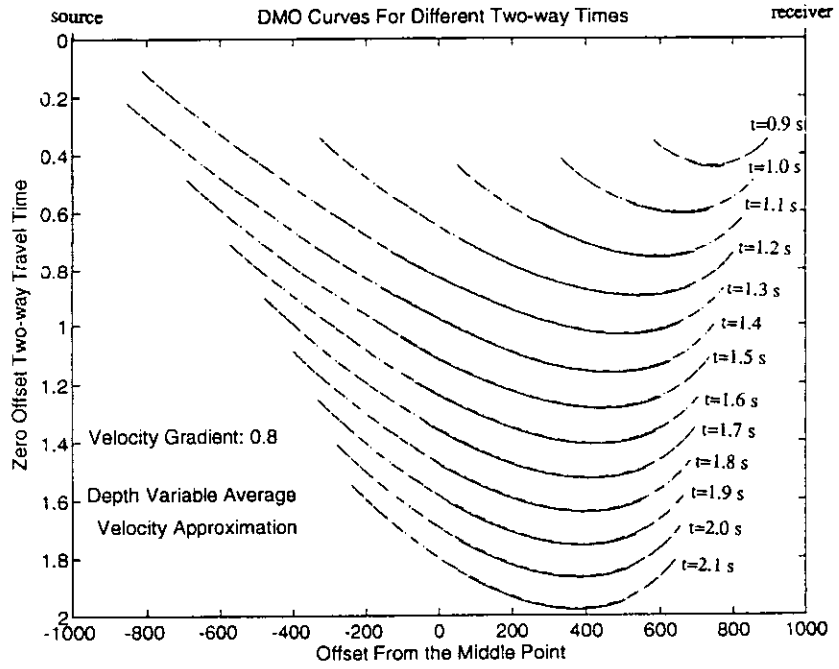

FIG. 10. *P-SV* DMO curves calculated using constant velocity DMO operator with approximated RMS (dash lines) and average (dash-dot lines) velocities at the depth of conversion point, as discussed in this paper. Solid lines are for accurate DMO operator. V_{p0}=3000 m/s, V_{s0}=1500 m/s, 2h=2000 m, $\alpha_{max}=80^0$ and k=0.8

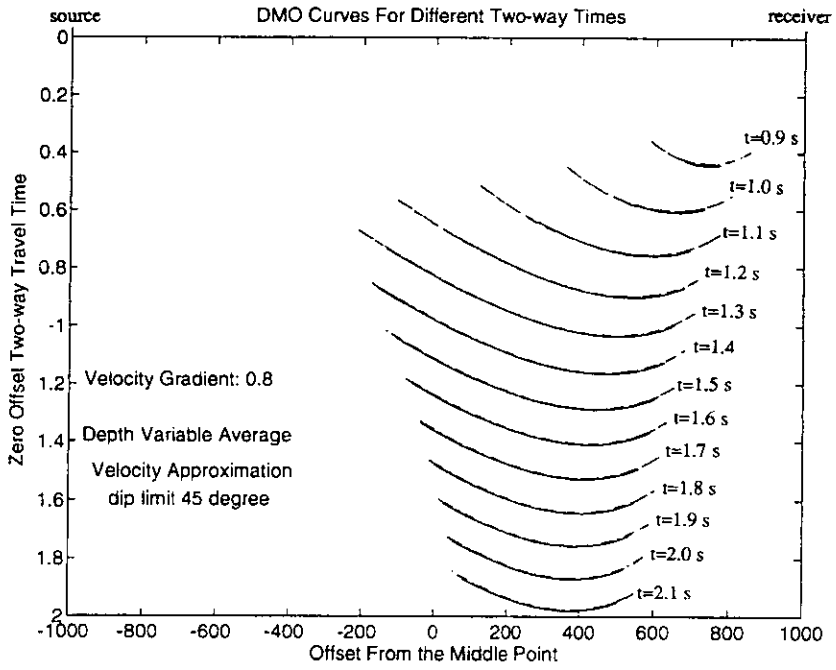

FIG. 11. *P-SV* DMO curves calculated using constant velocity DMO operator with approximated RMS (dash line) and average (dash line) velocities at the depth of conversion point, as discussed in this paper. Solid lines are for accurate DMO operator. V_{p0}=3000 m/s, V_{s0}=1500 m/s, 2h=2000 m and k=0.8

$\alpha_{max}=80^0$ and $\alpha_{max}=45^0$ for accurate and approximated DMO operators respectively.